Int. J. Heat Mass Transfer. Vol. 35, No. 6, pp. 1441–1453, 1992
Printed in Great Britain

0017–9310/92 $5.00 + 0.00

Numerical simulation of fluid flow and heat transfer in a thin liquid film over a rotating disk

M. M. RAHMAN and A. FAGHRI
Department of Mechanical and Materials Engineering, Wright State University, Dayton, OH 45435, U.S.A.

(*Received* 3 *January* 1991 *and in final form* 30 *May* 1991)

Abstract—The results of a numerical simulation of the flow field and associated heat transfer coefficient are presented for the free surface flow of a thin liquid film adjacent to a horizontal rotating disk. The computation has been performed for different flow rates and rotational velocities using a three-dimensional boundary-fitted coordinate system. Since the geometry of the free surface is unknown and dependent on flow rate, rate of rotation, and other parameters, an iterative procedure had to be used to ascertain its location. The computed film height agreed well with existing experimental measurements. The flow was dominated by inertia near the entrance and close to the free surface and dominated by centrifugal force at larger radii and adjacent to the disk. The rotation enhanced the heat transfer coefficient by a significant amount.

INTRODUCTION

THE FREE surface flow of a thin liquid film adjacent to a rotating surface is an interesting fluid mechanics problem since a number of surface and body forces act on the system simultaneously to shape the flow structure. The most dominant of these forces are: the friction exerted by the disk; the centrifugal and Coriolis forces due to rotation of the disk; and the inertia from the incoming fluid stream. This kind of flow is also quite commonly encountered in engineering processes, e.g. evaporation or condensation on a turbine blade and spin coating of metals. The primary motivation of this study, however, is to understand the fluid flow and heat transfer in a proposed absorber unit for a space-based vapor absorption refrigeration system. This kind of system is expected to be very useful in a micro-gravity environment where the centrifugal body force can be an effective driving mechanism for thinning the film to promote the absorption of the refrigerant vapor into the absorbent.

The fluid motion adjacent to a rotating surface in an infinite quiescent fluid medium is one of the fundamental problems in viscous fluid flow. Von Karman [1] presented an exact solution of the Navier–Stokes equation for this case by estimating the thickness of the boundary layer from a basic mass and momentum balance and developing a similarity variable to transform the partial differential equations for the conservation of mass and momentum to a set of ordinary differential equations. An integral method was used to solve the reduced equations. Later Sparrow and Gregg [2] extended the ideas of Von Karman to study the flow field and heat and mass transfer adjacent to a rotating disk in the presence of blowing or suction at the wall. The reduced transport equations were integrated numerically across the thickness of the boundary layer to determine radial, axial and tangential velocities and temperature and concentration distributions in dimensionless form. Results were presented for a range of positive and negative blowing rates as well as for the case of no blowing or suction.

In the present study, however, we are not concerned with boundary layer flow in an infinite medium of fluid, but the flow of a thin film adjacent to a plate. The boundary layer, however, develops within this thin liquid film and may extend all the way across the film. An analytical solution for the flow of a thin film adjacent to a rotating disk was presented by Rauscher *et al.* [3]. An asymptotic expansion technique was used where the radial spread of fluid was perturbed to determine the effects of convection, Coriolis acceleration, radial diffusion, surface curvature and surface tension. These higher-order effects were discussed on a physical basis. Their solution was valid for laminar flow with small Rossby number.

Espig and Hoyle [4] experimentally studied the surface waves in a thin liquid layer on a rotating disk. To correlate the experimental data, Nusselt's equation for film thickness on an inclined plate was modified to develop an expression for average film thickness, taking into account the effects of rotation. The thickness was found to be a function of volumetric flow rate, fluid viscosity and angular velocity of the disk. Needham and Merkin [5] studied the development of non-linear waves on the surface of a horizontally rotating thin liquid film. Using an asymptotic expansion technique, they studied the flow of a film much smaller in thickness than the distance from the axis of rotation. This distance, in turn, was smaller compared to the total radius of the disk in order to eliminate any end effects. It was found that the thickness of the film changed rapidly near the entrance due to spreading, while further away from the inlet, the film height was mainly determined by the centrifugal force

NOMENCLATURE

F	non-dimensional velocity in the radial direction, equation (12)
$\mathbf{g}$	gravitational acceleration, $-9.81\mathbf{j}$ [m s^{-2}]
G	non-dimensional velocity in angular direction, equation (13)
h	convective heat transfer coefficient, $q_w/(T_w - T_b)$ for heating; $q_w/(T_w - T_{sat})$ for evaporation [W m^{-2} K^{-1}]
$\mathbf{i}$	unit vector in the angular direction
$\mathbf{j}$	unit vector in the direction normal to the plate
k	cell index in the radial direction
$\mathbf{k}$	unit vector in the z-direction
K	thermal conductivity [W m^{-1} K^{-1}]
n	coordinate normal to the free surface, or number of grid cells in the radial direction
Nu	Nusselt number, $h\delta/K$
p	static pressure [Pa]
p_0	ambient pressure [Pa]
Pr	Prandtl number
q	heat flux [W m^{-2}]
Q_{in}	volumetric flow rate at the entrance [m^3 s^{-1}]
Q_{loss}	local rate of volume loss at a cell next to free surface [m^3 s^{-1}]
r	radial coordinate [m]
t	time [s]
T	temperature [K]
u	velocity in angular direction [m s^{-1}]
v	velocity in the direction normal to the plate [m s^{-1}]
$\mathbf{V}$	velocity vector [m s^{-1}]
w	velocity in the z-direction [m s^{-1}]
W_{in}	average radial velocity at entrance [m s^{-1}]
x	coordinate in angular direction [m]
y	coordinate normal to the plate [m]
z	coordinate in the radial flow direction (Fig. 1) [m].

Greek symbols

α	thermal diffusivity [m^2 s^{-1}] or relaxation factor
δ	film thickness [m]
ζ	non-dimensional coordinate perpendicular to the plate, equation (11)
ν	kinematic viscosity [m^2 s^{-1}]
ρ	density [kg m^{-3}]
τ	shear stress [N m^{-2}]
ω	angular velocity [rad s^{-1}].

Subscripts

b	mixed mean (bulk)
in	entrance
out	exit
r	component in radial direction
sat	saturation
w	solid wall
ϕ	component in the angular direction.

and viscous stress. An expression for film thickness was presented, which appears to be the same as that developed by Espig and Hoyle [4].

The analysis of evaporation of a thin liquid film from a rotating surface was presented by Butuzov and Rifert [6]. A closed-form solution of the film thickness was derived by neglecting inertia and making a basic balance of the centrifugal and frictional forces acting on the film. Bornside *et al.* [7] also studied evaporation from the free surface of a thin liquid film with reference to spin coating processes. A one-dimensional flow model was developed that accounted for variations in concentration, viscosity and diffusivity across the thickness of the spin coated film. The flow of the liquid was governed by a balance between the centrifugal driving force and the viscous resisting force. The equations of the flow and transport were solved using the Galerkin finite element method.

In all the above-mentioned studies, the thin film was primarily driven by centrifugal force. The inertia of the incoming fluid was either negligible or assumed to be so. In a space-based absorption refrigeration system, however, the film is expected to be introduced at the center of the disk with a significant amount of inertia to have a continuous flow of absorbent on the disk. This kind of system, where liquid is introduced at the center of the disk from a pressurized container and driven both by inertial and centrifugal forces, was studied recently by Thomas *et al.* [8, 9].

Thomas *et al.* [8] presented the numerical solution of the one-dimensional radial flow of a thin liquid film adjacent to a stationary and rotating disk. The continuity and momentum equations were integrated across the thickness of the film by assuming a flat velocity profile to develop a single equation for film velocity. The resistance to the flow due to wall shear stress was expressed in terms of an empirical friction coefficient which was estimated from the radial flow velocity. The thickness of the film was predicted by solving the equation for film velocity as a transient problem using the MacCormack predictor–corrector method.

Thomas *et al.* [9] presented experimental measurements of radially spreading flow of a thin film adjacent to a horizontal disk. A non-obtrusive capacitance technique was used for the measurement of the film

height distribution. A photographic study was done to understand the nature of the surface waves. Tests were performed both for stationary and rotating disks at flow rates ranging from 7 to 15 l.p.m. The rate of rotation varied between 0 and 300 r.p.m. Their experiments predicted the presence of a hydraulic jump when the disk was stationary. The jump moved downstream with an increase of the flow rate and rotational velocity. Waves were found to be present on the free surface at all flow rates and rates of rotation.

The present study is undertaken to develop a computational procedure for solving the governing transport equations in their complete three-dimensional form for the flow of a thin liquid film adjacent to a rotating disk. This methodology eliminated the need for assuming a friction coefficient as was done in the one-dimensional model developed by Thomas *et al.* [8]. Furthermore, an attempt is also made to improve the simple one-dimensional solution procedure. All computed results are compared with the experimental measurements of Thomas *et al.* [9]. The details of the three-dimensional flow field and distribution of the heat transfer coefficient are discussed.

MATHEMATICAL MODEL

The curvilinear boundary-fitted coordinate system used for the three-dimensional numerical computation is shown in Fig. 1. The local coordinates are directed along lines connecting the centers of the adjacent grid cells. The x-axis is directed in the azimuthal direction, the y-axis perpendicular to the plate and the z-axis along the radial flow direction. The velocity components in these three directions are u, v and w, respectively. Due to the axisymmetric nature of the flow and vertical entrance and exit sections, u is directed parallel to the plate and v is directed perpendicular to the plate. However, w changes its direction along the plate depending on the slope of the free surface. The height of the free surface from the solid wall is denoted by δ, which varies with radial location.

For incompressible flow with constant fluid properties, the equations for the conservation of mass, momentum, and energy are given by

$$\nabla \cdot \mathbf{V} = 0 \tag{1}$$

$$\frac{\mathrm{D}\mathbf{V}}{\mathrm{D}t} = -\frac{1}{\rho}\nabla p + \nu\nabla^2\mathbf{V} + \mathbf{g} \tag{2}$$

$$\frac{\mathrm{D}T}{\mathrm{D}t} = \alpha\nabla^2 T. \tag{3}$$

The terms due to viscous dissipation and pressure work in the energy equation are neglected, as is typical for any low speed flow. Since the flow is symmetric about the axis of rotation, there was no variation of velocity or temperature in the angular direction, i.e. $\partial\mathbf{V}/\partial x = 0$ and $\partial T/\partial x = 0$. At the free surface, both tangential and normal stress components are zero. The vanishing tangential stress condition is represented by the zero velocity gradient on the free surface. The normal stress condition on the free surface leads to equations balancing the pressure and other stresses, including surface tension. Scaling these equations, one can show that, for a thin film flow where Weber and Reynolds numbers are large, all other stress terms are negligible compared to pressure, leading to $p = p_0$ on the free surface. The kinematic condition on the free surface relates the variation of film height to the velocity components. At the entrance plane, the velocity is assumed to be radial with a parabolic profile. At the exit plane, the flow is assumed to be fully developed with a hydrostatic pressure profile. In general, the velocity and temperature information at the exit is unknown, but needs to be specified for an elliptic problem. Since the flow becomes entirely supercritical for the rotational

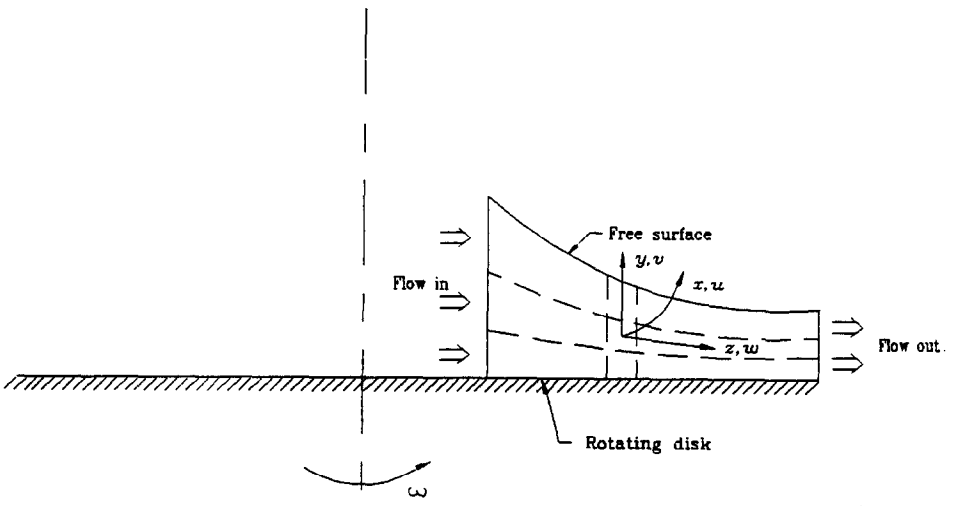

FIG. 1. Schematic of the flow of a thin liquid film adjacent to a rotating disk.

speeds considered here, the solution is not very sensitive to the exit boundary condition, and vanishing gradients for velocity and temperature are appropriate. The boundary conditions for the flow considered here are then given by

at $y = 0$:

$$\mathbf{V} = \omega r\mathbf{i}, \quad T = T_w \tag{4}$$

at $y = \delta$:

$$\frac{\partial \mathbf{V}}{\partial n} = 0, \quad p = p_0, \quad \frac{d\delta}{dz} = \frac{v}{w},$$

$$\begin{cases} \dfrac{\partial T}{\partial n} = 0, & \text{heating} \\ T = T_{sat}, & \text{evaporation} \end{cases} \tag{5}$$

at $z = r_{in}$:

$$\mathbf{V} = 1.5\, W_{in}\left[2\left(\frac{y}{\delta}\right) - \left(\frac{y}{\delta}\right)^2\right]\mathbf{k},$$

$$T = T_{in} \tag{6}$$

at $z = r_{out}$:

$$\frac{\partial \mathbf{V}}{\partial z} = 0, \quad p = p_0 + \rho \mathbf{g}(\delta - y),$$

$$\frac{\partial T}{\partial z} = 0. \tag{7}$$

Here n is the direction normal to the free surface. The quantities T_w, T_{sat}, T_{in}, W_{in} and ω are assumed to be constant. Two different thermal conditions are considered on the free surface: simple heating without evaporation and evaporation. For the first case, the free surface is assumed to be adiabatic in nature. In the second case, the free surface is isothermal at its equilibrium saturation temperature, T_{sat}. In the present investigation it is also assumed that, in the case of evaporation, the fluid enters at its equilibrium saturation temperature, i.e. $T_{in} = T_{sat}$. The Nusselt number is defined in terms of film thickness since that is the most significant length scale for this problem.

COMPUTATIONAL PROCEDURE

Three-dimensional method

The governing transport equations, along with the boundary conditions described in the previous section, were solved numerically using a boundary-fitted curvilinear coordinate system. The irregular free surface was taken as one of the boundaries of the computational domain. The solution domain was pie-shaped, extending from r_{in} to r_{out} in the radial direction and over a small angle in the angular direction in order to prevent both distortion of body-fitted coordinates at large radii and clustering of grids at smaller radii. The grid cells were generated by an algebraic interpolation between the boundaries of the domain. In general, the cell faces were non-orthogonal to each other. As shown in Fig. 1, the local coordinates were defined along lines connecting the centers of the adjacent grid cells. The x-axis was taken in the azimuthal direction, the y-axis perpendicular to the plate and the z-axis in the radial flow direction. The velocity resolutes in these three directions are u, v, and w, respectively. In the finite difference formulation, the co-variant components, i.e. components parallel to the cell faces, were used to represent the velocity and force vectors.

The finite difference equations were derived by using the principle of conservation of mass, momentum and energy at each cell. The primary variables were preserved in the formulation instead of non-dimensionalizing. The quantities were stored in a staggered fashion where they made more physical sense for cell conservation. For each cell, the velocity components were stored at downstream boundaries, whereas all pressures and temperatures were stored at the cell center. The mass flux across a cell boundary was computed exactly from the scalar product of the velocity vector and the vector representing the area of the cell face. The convection contributions to a cell from its neighbors were calculated exactly by taking into account the curvature of a cell face and its non-orthogonal orientation. In the calculation of diffusion, however, the cell boundaries were approximated to be locally orthogonal. The hybrid difference scheme demonstrated by Patankar [10] was used to preserve the relative contribution of convection and diffusion to a cell from its neighbor in terms of cell Peclet number. This is a common practice in the computation of convective flows.

The distribution of cells in the computational domain was determined from a series of tests with different numbers of cells in the x, y, and z directions. Due to the axisymmetric nature of the flow, only five cells with an angular extent of 2.3° cell were found to be adequate in that direction. This provided a total angle of 11.5° for the entire computational domain. Test runs with 3.45° cell and 2.3° cell yielded heat transfer coefficients within 0.001%. Similarly, runs with two cells and five cells in the angular direction resulted in heat transfer coefficients within 0.0005%. Similar tests for the other two directions showed that 50 cells in the radial direction and 30 cells across the thickness of the film resulted in grid-independent solutions. Therefore, the computational domain was divided into $5 \times 30 \times 50$ cells by simple algebraic interpolation to generate a uniformly distributed grid structure.

The finite difference equations were solved by using the SIMPLEST algorithm as presented by Spalding [11], which is an iterative solution procedure where the computation was started by guessing a pressure field. Then the momentum equations were solved to determine the velocity components. The pressure was updated using the continuity equation. Even though the continuity equation does not contain any pressure, it can be easily transformed to a pressure correction equation as shown by Patankar [10]. The iterations were continued until the sum of the residuals for all computational cells dropped below 10^{-6} for each

equation. Since the flow was not coupled to the thermal transport for the problem considered here, the temperature field was solved once the film height distribution was completely ascertained.

Since the geometry of the free surface was dependent on the flow parameters, but needed to be specified to generate the grid structure for the three-dimensional computation, an iterative procedure had to be used to ascertain the location of the free surface. The free surface boundary was assumed to be a permeable wall through which fluid particles were allowed to enter or leave the computational domain. Since the ambient pressure was prescribed, an outflow took place when the static pressure of the fluid adjacent to the free surface was higher than the ambient pressure and vice versa. The penetration of fluid through the free surface essentially violated the kinematic condition on the surface, which was arrived at by adjusting the surface height distribution in successive iterations. The scheme worked as follows:

(1) A free surface height distribution was prescribed (based on the one-dimensional solution of Thomas *et al.* [8] or any improved method).

(2) The flow field was solved completely for that height distribution.

(3) The amount of penetration of the fluid through the surface was calculated at all locations along the flow:

$$(Q_{\text{loss}})_k = Q_{k-1} - Q_k.$$

(4) The new free surface height was determined from the old height and the rate of penetration:

$$(\delta_{\text{new}})_k = (\delta_{\text{old}})_k + \alpha \frac{(Q_{\text{loss}})_k}{Q_{\text{in}}} (\delta_{\text{old}})_k$$

where α is the relaxation factor.

(5) Iterations were continued until the rate of penetration became negligible.

For a given surface height distribution, the deviation from the ideal zero penetration condition was estimated by the following measures.

(a) Root-sum-square penetration

$$= \frac{\sqrt{\left(\sum_{k=1}^{n} (Q_{\text{loss}})_k^2\right)}}{Q_{\text{in}}}. \tag{8a}$$

(b) Absolute sum of penetration

$$= \frac{\sum_{k=1}^{n} |(Q_{\text{loss}})_k|}{Q_{\text{in}}}. \tag{8b}$$

(c) Maximum error in flow rate

$$= \frac{|(Q - Q_{\text{in}})|_{\max}}{Q_{\text{in}}}. \tag{8c}$$

All these quantities were found to decrease almost monotonically with iterations. The final results presented here had both absolute sum of penetration and maximum error in flow rate of less than 0.06 and root-sum-square penetration less than 0.02. A relaxation factor of $\alpha = 1$ (i.e. no relaxation) was found to be adequate in most computations. Since the flow field was not affected by thermal transport, the energy equation was solved only for the final free surface height distribution with no penetration through the surface. The above computational algorithm is termed as the porous wall method originally outlined by Rahman *et al.* [12]. Significant modifications of the method, however, have been made here to improve the iteration procedure as well as the error estimates. Moreover, this is the first time it has been applied to predict three-dimensional flow involving rotation.

Improved one-dimensional method

The one-dimensional computational procedure, developed by Thomas *et al.* [8], was also improved here by incorporating a better estimate of frictional resistance exerted by the solid wall on the flow. In the one-dimensional method, the governing equations for mass and momentum were integrated across the thickness of the film assuming a uniform velocity profile. In the original procedure of Thomas *et al.* [8], the flow was assumed to be strictly radial in nature with a superimposed solid-body rotation. The resistance to the flow due to friction was taken to be the resistance in the radial direction. In the azimuthal direction, the velocity remained constant across the thickness of the film with no resistance from the solid wall. In reality, however, the velocity is expected to change due to the finite viscosity of the fluid, so there will be frictional resistance from the wall in the azimuthal direction. To account for the frictional resistance due to the angular velocity, we may define the total shear stress as

$$\tau_w = \sqrt{(\tau_\phi^2 + \tau_r^2)}. \tag{9}$$

Here $\tau_r = c_f(1/2\rho W^2)$, where c_f can be calculated by using the Blasius [13] solution or the parabolic solution given by Rahman *et al.* [14]. Also, τ_ϕ can be estimated from the exact solution of laminar flow adjacent to a rotating disk in an infinite extent of fluid [15]:

$$\tau_\phi = 0.6\rho r v^{1/2} \omega^{3/2}. \tag{10}$$

Using τ_w as the shear stress at the solid wall, the discretized equations of Thomas *et al.* [8] were reformulated and solved to give the film height distribution for any given flow rate and rate of rotation.

RESULTS AND DISCUSSION

The three-dimensional computational procedure discussed in the previous section was first tested against the limiting flow situations, where theoretical or experimental results are available. By setting the rotational speed to zero, the computed results reproduced exactly the film height distribution and velocity field corresponding to two-dimensional thin film flow

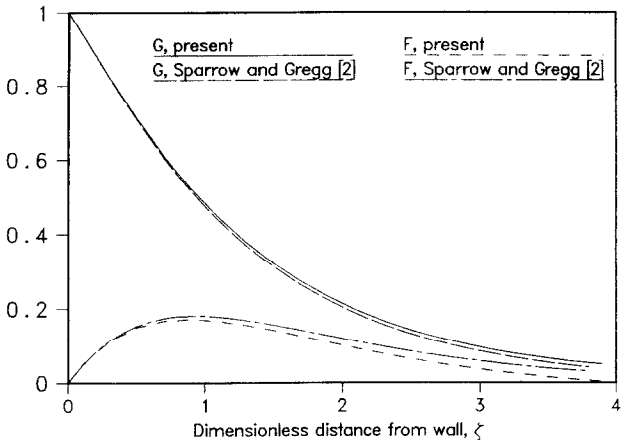

FIG. 2. Comparison of numerical results with similarity solution for fluid motion adjacent to a rotating disk in an infinite fluid medium.

adjacent to a stationary disk, as presented by Rahman *et al.* [12]. Another limiting case was the flow induced by a rotating disk in an otherwise stagnant infinite fluid medium. Analytical solutions for this case were developed by Von Karman [1] and later extended by Sparrow and Gregg [2]. In this system, the flow is limited to a thin boundary layer adjacent to the disk. The computed solution for this limiting case is presented in Fig. 2, where it is compared with the analytical results presented in ref. [2] for no blowing or suction at the wall. The non-dimensional distance, ζ, and velocity components G and F are defined as

$$\zeta = y\sqrt{\left(\frac{\omega}{\nu}\right)} \tag{11}$$

$$F = \frac{w}{r\omega} \tag{12}$$

$$G = \frac{u}{r\omega}. \tag{13}$$

Both the radial and azimuthal velocity distributions across the thickness of the boundary layer are reasonably matched. One major difference between the conventional boundary layer flow and the flow of a thin film is that the thickness of the film is finite and bounded by the free surface which interacts with the surrounding medium.

The height of a thin film adjacent to a rotating disk was experimentally measured by Thomas *et al.* [9]. A horizontal disk 406.4 mm in diameter was used for the experiment where water at 20°C was introduced radially through a slot 0.267 mm in height at a radial location of 50.8 mm. The film height was measured along the radius by using a non-obtrusive capacitance probe from 76.2 mm to 195.6 mm. The measurements were not reported past 195.6 mm because part of the capacitance sensor was over the edge of the disk. Twenty sets of experimental data were taken covering flow rates of 7–15 l.p.m. and rotational speeds of 55–300 r.p.m. The flow was isothermal and no measurement of heat transfer was done in that experiment. In the present investigation, we used the flow and rotation conditions presented by Thomas *et al.* [9], so that a relative comparison of the film height distribution could be made. The specific cases chosen here are listed in Table 1. Prediction of film height and heat transfer coefficient could be done for all the experimental runs. However, to save the computational efforts, some specific cases were picked to cover the range of experiments in terms of flow rate and rate of rotation, as well as to understand the trend of the variation of the flow field and heat transfer coefficient with flow rate and rotational speed. The table also lists the root-sum-square penetration, absolute sum of penetration and maximum error in

Table 1. Flow and rotation rates in the present investigation

Case No.	Flow rate (l.p.m.)	Rotational speed (r.p.m.)	Root square penetration	Absolute sum of penetration	Maximum error in flow rate
1	9	200	0.0043	0.0199	0.0113
2	15	200	0.0072	0.0235	0.0152
3	7	100	0.0050	0.0258	0.0152
4	11	100	0.0110	0.0406	0.0218
5	15	300	0.0020	0.0097	0.0076
6	15	55	0.0127	0.0593	0.0540
7	7	300	0.0148	0.0445	0.0100
8	15	100	0.0092	0.0332	0.0224

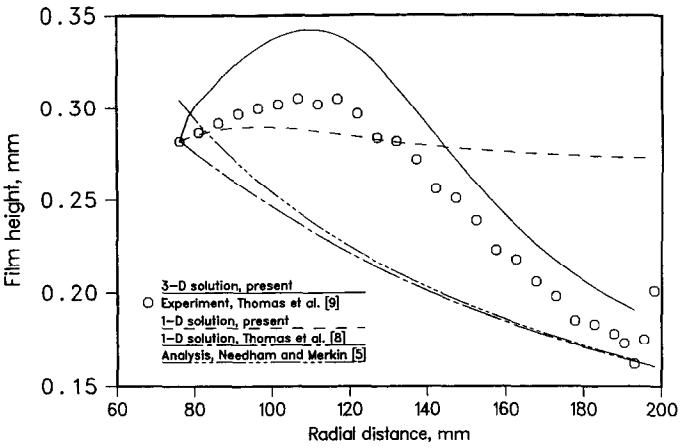

FIG. 3. Comparison of numerical solution with experimental data for thin liquid film at a flow rate of 9 l.p.m. and angular velocity of 200 r.p.m.

flow rate corresponding to the three-dimensional film height distribution for each specific flow rate and rate of rotation. For computational runs involving heat transfer, the wall temperature is assumed to be 30°C, whereas the entering fluid (water) is at 10°C. This gave a film temperature of 20°C for the evaluation of properties.

The computed film height for a flow rate of 9 l.p.m. and rotational speed of 200 r.p.m. (case 1 in Table 1) is shown in Fig. 3. The experimental data as well as the computed results using previous one-dimensional solution algorithms are also shown in the same figure. The three-dimensional solution predicted the trend of the experimental data, i.e. the film height first increased, attained a peak and then decreased further downstream. The increase of the film height near the entrance is due to the strong frictional resistance the flow encounters from the solid wall. However, as the radius increased, the centrifugal force increased in magnitude and overpowered the frictional resistance. Then the film height decreased due to the increase in flow velocity as well as radial spreading. The effect of radial spreading was more significant at smaller radii. At larger radii, the curvature decreased and radially spreading flow approached plane flow. The one-dimensional solution of Thomas *et al.* [8] shows a monotonic decrease of film height with radius, and the height is consistently underpredicted except very close to the exit. Thomas *et al.* [8] assumed a solid-body rotation condition with no variation of velocity across the thickness of the film. Moreover, friction was computed based on the radial velocity using an empirical correlation. Therefore, the centrifugal force was more and frictional force was less accounted for in the numerical formulation. Therefore, the trend seen here is quite expected. The modified one-dimensional solution presented here improved the prediction of film height at smaller radii, but failed to do so at large radii. Here both radial and azimuthal components of frictional forces were accounted for, but still keeping no velocity variation across the thickness of the film. It may be noticed that the present three-dimensional solution, unlike the one-dimensional methods, does not require any estimate of the friction coefficient. Figure 3 also shows a comparison with the analysis of Needham and Merkin [5]. Since the analysis presented an asymptotic solution valid for solid-body rotation, the analytical solution shows a monotonic decrease in film height and compared well with the computation of Thomas *et al.* [8], where similar assumptions were incorporated. In reality, however, viscous resistance at the wall slowed the film and resulted in a larger height distribution. Moreover, the asymptotic solution neglected the effects of inertia which were significant in the experiment and were adequately accounted for in the three-dimensional solution. The computed results for a rotational rate of 200 r.p.m. and flow rate of 15 l.p.m. (case 2 in Table 1) are shown in Fig. 4. Here, the present three-dimensional solution gives a very good agreement with the experimental data. The one-dimensional algorithm of Thomas *et al.* [8] consistently underpredicted the film height whereas the present one-dimensional algorithm improved it somewhat, particularly near the entrance and exit. The analytical solution of Needham and Merkin [5] showed a large film height near the entrance that monotonically decreased downstream. Near the entrance, the flow was dominated by inertia, and therefore the analytical results of Needham and Merkin [5] were not valid in that region.

The film height at a rotational rate of 100 r.p.m. for two different flow rates (cases 3 and 4 in Table 1) is shown in Figs. 5 and 6. At this rate of rotation, the one-dimensional solution procedure using the resultant frictional resistance gave a reasonable overall agreement, whereas the procedure of Thomas *et al.* [8] still underpredicted the film height at most locations. The analytical solution, as before, overpredicted the film height at smaller radii and underpredicted it at larger radii. The present three-dimensional solution gave the best agreement with the exper-

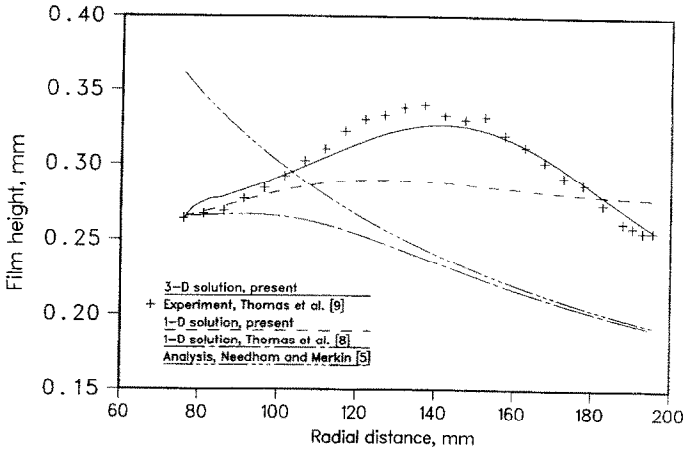

FIG. 4. Comparison of numerical solution with experimental data for thin liquid film at a flow rate of 15 l.p.m. and angular velocity of 200 r.p.m.

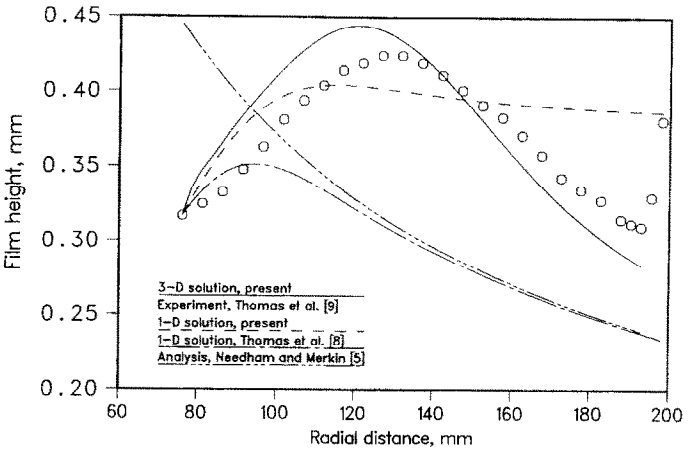

FIG. 5. Comparison of numerical solution with experimental data for thin liquid film at a flow rate of 7 l.p.m. and angular velocity of 100 r.p.m.

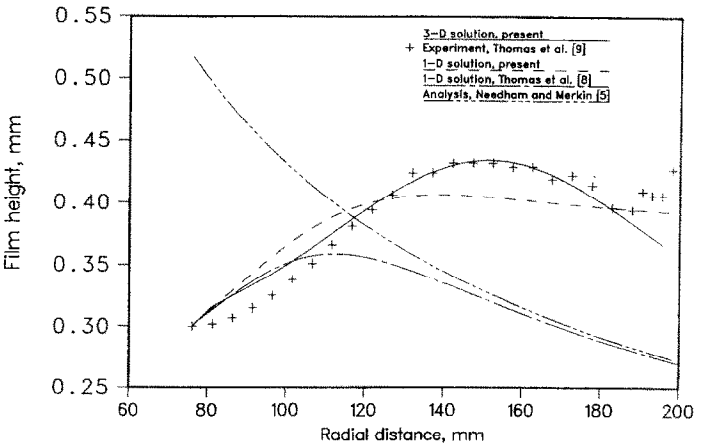

FIG. 6. Comparison of numerical solution with experimental data for thin liquid film at a flow rate of 11 l.p.m. and angular velocity of 100 r.p.m.

imental data even though it did not coincide with it. A small overestimate of the film height near the entrance may be due to the development of the velocity profile from the given entrance boundary condition. At this boundary, the velocity was assumed to be parabolic in nature with a maximum on the free surface. This is the best condition one can impose for laminar flow, as confirmed from the distribution of

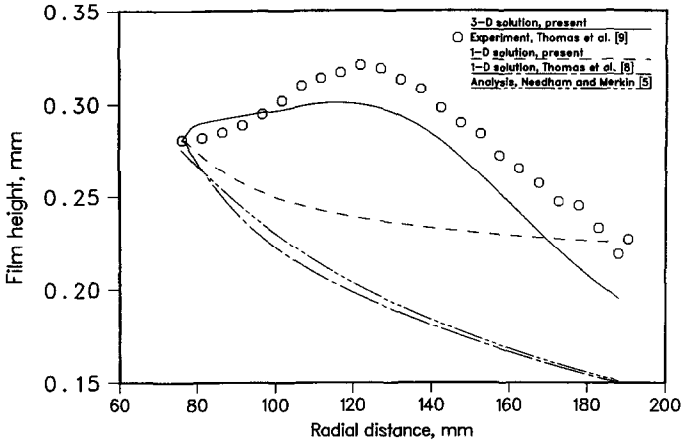

FIG. 7. Comparison of numerical solution with experimental data for thin liquid film at a flow rate of 15 l.p.m. and angular velocity of 300 r.p.m.

velocity across the thickness of the film in an intermediate location of the flow.

The distribution of the film height for 300 r.p.m. and flow rate of 15 l.p.m. (case 5 in Table 1) is shown in Fig. 7, where it is compared with the one-dimensional predictions of Thomas *et al.* [8], the experimental data of Thomas *et al.* [9] and the analysis of Needham and Merkin [5]. In this situation, the numerical solution underpredicted the experimental data in most regions. The one-dimensional algorithm of Thomas *et al.* [8] produced a film height distribution that was much smaller than the experimentally measured values. The present one-dimensional algorithm improved it further, whereas the present three-dimensional solution compares best with the experimental data. The trend of the data that the film height first increased, attained a peak and then decreased downstream was captured only by the present three-dimensional numerical solution. The one-dimensional solutions for this case show a monotonic decrease of film height with radius. The analysis of Needham and Merkin [5] compared better with the computation of Thomas *et al.* [8] at a larger rate of rotation since the effects of inertia became smaller. The above comparisons (Figs. 3–7) show that the present algorithm can be an effective means for the prediction of the film height for a thin film flow adjacent to a rotating disk. The small deviations from the experimental values are within the uncertainties of experimental measurements and can also be attributed to unsteady surface waves as well as the surface tension effects that were not accounted for in the present steady-state numerical formulation, especially at the outer edge of the disk where the experimental data showed an increase in film height.

The distributions of the velocity vectors at three locations across the film are shown in Figs. 8 and 9, respectively, for two limiting operating conditions: case 6 (55 r.p.m., 15 l.p.m.) and case 7 (300 r.p.m., 7 l.p.m.). In Fig. 8, at $y/\delta = 0.82$ the velocity was almost radial near the entrance and turned by a small angle as the flow moved downstream. Since the flow rate

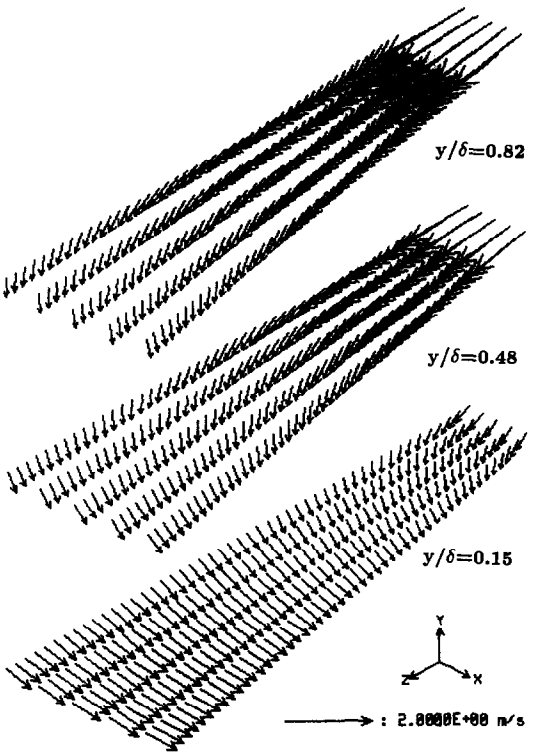

FIG. 8. Velocity vectors for thin liquid film at a flow rate of 15 l.p.m. and angular velocity of 55 r.p.m.

was high compared to the rate of rotation, the flow near the free surface was dominated by the entrance condition. At $y/\delta = 0.15$, which was near the solid wall, the velocity vectors were directed more in the angular direction, particularly at larger radii. Looking at the magnitude of the velocity vectors, the centrifugal force increased as the radius increased. At $y/\delta = 0.48$, the velocity vectors turned at an angle that increased with radial distance. Also, the overall magnitude of the vectors decreased with radius due to the resistance exerted by the solid wall. At smaller

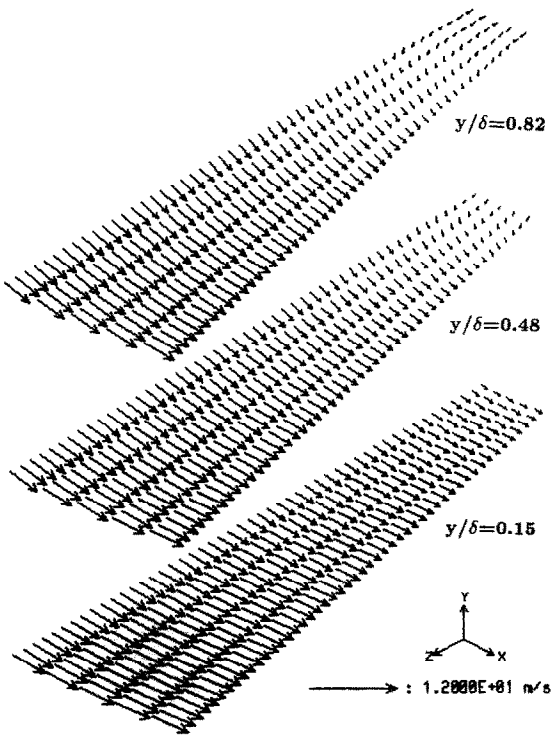

FIG. 9. Velocity vectors for thin liquid film at a flow rate of 7 l.p.m. and angular velocity of 300 r.p.m.

radii, the velocity increased with distance from the wall since frictional resistance became smaller. At larger radii, however, an opposite trend was seen due to the stronger centrifugal force that accelerated fluid particles near the wall. The flow was dominated by inertia at smaller radii and at locations away from the wall, whereas the contribution of rotation became important at locations near the solid wall and in regions away from the center. From a plot of the velocity components in the radial and azimuthal directions, it was found that the profile for w was approximately parabolic in nature with a maximum at the free surface and zero at the wall. This corroborates corresponding observations for a stationary disk presented by Rahman *et al.* [12]. The azimuthal component was maximum at the solid wall and gradually decreased nearer the free surface. The normal component of velocity was found to be small compared to either of these components.

In Fig. 9, the flow was dominated by rotation in most regions except near the entrance when the rotational speed was 300 r.p.m. and the flow rate was 7 l.p.m. At this condition, the inertia was overpowered by the high rotational velocity after traversing some distance. Looking at the magnitude, the resultant velocity increased with radius. At intermediate flow rates and rates of rotation, the vector plots showed behavior within these two limits. The effect of the flow rate was found to increase the radial component of velocity, whereas rotation increased both radial and azimuthal components. The friction always counteracted these velocities to arrive at an equilibrium condition. The fluid particles exited the disk at an angle with the radial direction that increased with the rate of rotation.

A plot of Nusselt number for a flow rate of 15 l.p.m. at two different rates of rotation is shown in Fig. 10 (cases 5 and 8 in Table 1). The plots correspond to two different thermal boundary conditions on the free surface; namely, simple heating without evaporation, when the free surface is approximately adiabatic in nature, and an evaporative free surface when the surface is isothermal at the equilibrium saturation temperature. The thermal condition at the rotating disk surface is assumed to be a uniform temperature higher than the entering fluid temperature. The Nusselt number decreased rapidly near the entrance at all flow and heating conditions. This was due to the development of the thermal boundary layer as the fluid moved downstream. For both the cases of heating and evaporation, the Nusselt number for the case of 300 r.p.m. decreased monotonically all the way to the exit, whereas in the case of 100 r.p.m., the Nusselt number first decreased, attained a minimum and then increased further downstream to approach an approximately constant value near the exit. The Nusselt number for heating was consistently higher than the corresponding case of evaporation at all radial locations and all rates of rotation. This was also observed in connection with heat transfer to a falling liquid film presented by Seban and Faghri [16]. The Nusselt number for 300 r.p.m. was higher than that for 100 r.p.m. in most regions of the disk except close to the exit. The slightly higher Nusselt number near the exit was due to a much larger film height than the corresponding case of 300 r.p.m. An overall enhancement of Nusselt number is obtained by increasing the rate of rotation.

The Nusselt number here is defined in terms of local film thickness, which varies along the radius. The film thickness also decreased as the rotational velocity increased. To see the distribution of the heat transfer rate more clearly, the values of the heat transfer coefficient for the same flow rate and heating conditions are shown in Fig. 11. The heat transfer coefficient for 300 r.p.m. was consistently higher than that for 100 r.p.m. at all radial locations. This is quite expected since the rate of rotation increased the centrifugal force which accelerated and thinned the film, both of which contributed to the enhancement of heat transfer. For the case of 300 r.p.m. and simple heating, the heat transfer coefficient decreased near the entrance, attained a minimum and then increased further downstream. For the other cases shown here, the heat transfer coefficient approached an approximately constant value after a gradual decrease near the entrance. As the radius increased, the inertial force decreased and centrifugal force increased, both of which were counteracted by frictional resistance at the solid wall. In the absence of rotation or any external

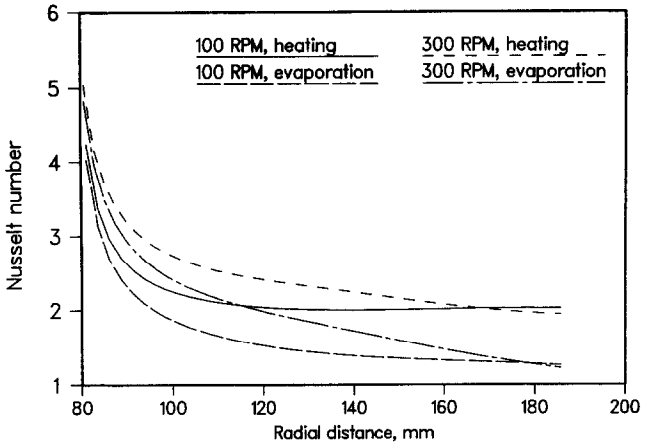

FIG. 10. Nusselt number distribution for thin liquid film at a flow rate of 15 l.p.m.

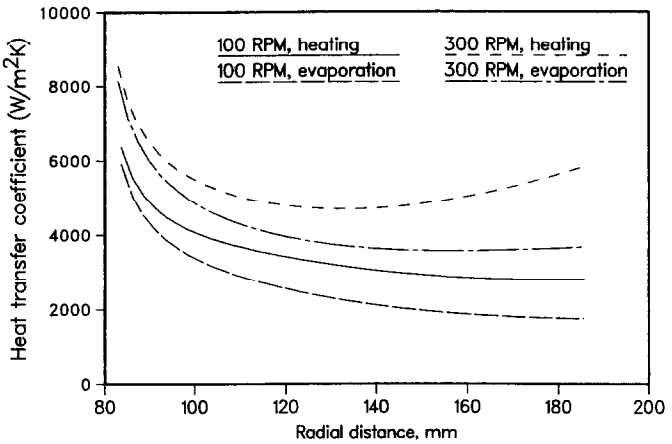

FIG. 11. Heat transfer coefficient for thin liquid film at a flow rate of 15 l.p.m.

body force, the heat transfer coefficient gradually decreased downstream as seen in the studies by Rahman *et al.* [12] for radial flow at zero gravity. The rotation balanced out or even overcame the frictional resistance at larger rates of rotation, as seen in the vector plot for 300 r.p.m. (Fig. 9). Therefore, the convective heat transfer, which is intimately related to the fluid velocity, increased downstream once the centrifugal force became the dominant driving mechanism. If a disk of larger radius was considered, we could possibly see a minimum followed by a gradual rise in the heat transfer coefficient for all cases. Also, the effects of rotation in the enhancement of the heat transfer coefficient were greater for the case of simple heating than the case of evaporation.

Figure 12 shows the variation of Nusselt number with radial distance for a given rate of rotation at different flow rates. For the case of 15 l.p.m., the Nusselt number monotonically decreased from the entrance radius, but for the case of 7 l.p.m., it decreased gradually at smaller radii and approached a constant value further downstream. The behavior is the same for the cases of heating and evaporation. For the disk considered here, the Nusselt number for 15 l.p.m. was higher than that for 7 l.p.m. at all radial locations. This is expected, particularly at smaller radial locations, since fluid velocity will be higher at larger flow rates. At large radii, however, when the effects of rotation become more important, a higher heat transfer coefficient may be attained by using a smaller flow rate due to greater thinning of the film. So, by controlling the disk radius, flow rate and rate of rotation, one may attain any desired requirement of heat transfer in this kind of flow system.

CONCLUSIONS

Numerically computed distributions of the film height, velocity vectors and heat transfer coefficient are presented for the free surface flow of a thin liquid film adjacent to a horizontal rotating disk. The flow was dominated by inertia at smaller radii and close to the free surface and dominated by rotation near the solid wall and at larger radii. The radial component of velocity had an approximately parabolic profile which was maximum at the free surface and zero at the solid wall. The angular component of velocity was maximum at the wall and gradually diminished across

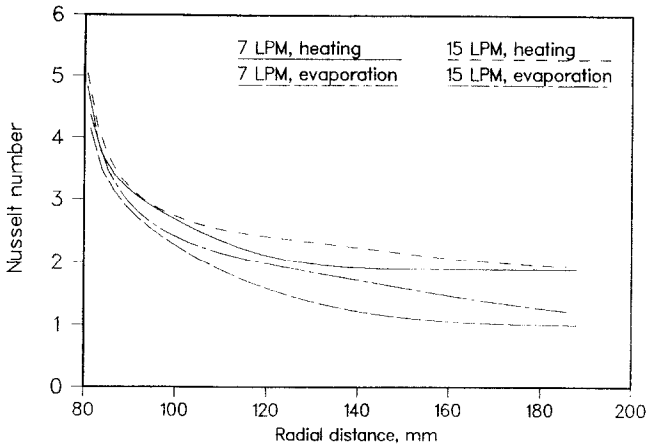

FIG. 12. Nusselt number distribution for thin liquid film at a rotation rate of 300 r.p.m.

the thickness of the film. The local fluid velocity increased with an increase in both the volumetric flow rate and angular velocity. The fluid particles exit the disk at an angle with radius that increased with the rate of rotation. At the flow rates and rates of rotation considered here, the film height first increased, attained a peak and then decreased further downstream. The increment of the film height is attributed to frictional resistance, whereas the reduction of the film height at larger radii is due to the spreading of the film as the flow area increases as well as the increase of the centrifugal force with radius. The predicted height using the present three-dimensional computational method agreed well with experimental measurements. The rate of heat transfer is enhanced by a significant amount by increasing the rate of rotation for both cases of simple heating with no evaporation and evaporation at the free surface.

Acknowledgement—Funding for this work was provided by the NASA Goddard Space Flight Center, Greenbelt, Maryland, under contract NAG5-956.

REFERENCES

1. T. Von Karman, Über Laminare und Turbulent Reibung, *Z. Angew. Math. Mech.* **1,** 233–235 (1921).
2. E. M. Sparrow and J. L. Gregg, Mass transfer, flow and heat transfer about a rotating disk, *ASME J. Heat Transfer* **82,** 294–302 (1960).
3. J. W. Rauscher, R. E. Kelly and J. D. Cole, An asymptotic solution for the laminar flow of a thin film on a rotating disk, *ASME J. Appl. Mech.* **40,** 43–47 (1973).
4. H. Espig and R. Hoyle, Waves in thin liquid layer on a rotating disk, *J. Fluid Mech.* **22,** 671–677 (1965).
5. D. J. Needham and J. H. Merkin, The development of nonlinear waves on the surface of a horizontally rotating thin liquid film, *J. Fluid Mech.* **184,** 357–379 (1987).
6. A. I. Butuzov and V. G. Rifert, Heat transfer in evaporation of liquid from a film on a rotating disk, *Heat Transfer—Sov. Res.* **5,** 57–61 (1973).
7. D. E. Bornside, C. W. Macosko and L. E. Scriven, Spin coating: one-dimensional model, *J. Appl. Phys.* **66,** 5186–5193 (1989).
8. S. Thomas, W. L. Hankey, A. Faghri and T. Swanson, One-dimensional analysis of the hydrodynamic and thermal characteristics of thin film flows including the hydraulic jump and rotation, *ASME J. Heat Transfer* **112,** 728–735 (1990).
9. S. Thomas, A. Faghri and W. L. Hankey, Experimental analysis and flow visualization of a thin liquid film on a stationary and rotating disk, *ASME J. Fluids Engng* **113,** 73–80 (1991).
10. S. V. Patankar, *Numerical Heat Transfer and Fluid Flow*. Hemisphere, New York (1980).
11. D. B. Spalding, Mathematical modeling of fluid mechanics, heat transfer and chemical reaction processes, a Lecture Course, CFDU HTS/80/1, Imperial College, London (1980).
12. M. M. Rahman, A. Faghri and W. L. Hankey, New methodology for the computation of heat transfer in free surface flows using a permeable wall, *Numer. Heat Transfer*, Part B **18,** 23–41 (1990).
13. W. M. Kays and M. E. Crawford, *Convective Heat and Mass Transfer* (2nd Edn). McGraw-Hill, New York (1980).
14. M. M. Rahman, W. L. Hankey and A. Faghri, Analysis of fluid flow and heat transfer in a thin liquid film in the presence and absence of gravity, *Int. J. Heat Mass Transfer* **34,** 103–114 (1991).
15. H. Schlichting, *Boundary Layer Theory* (7th Edn). McGraw-Hill, New York (1979).
16. R. A. Seban and A. Faghri, Evaporation and heating with turbulent falling liquid films, *ASME J. Heat Transfer* **98,** 315–318 (1976).

SIMULATION NUMERIQUE DE L'ECOULEMENT ET DU TRANSFERT THERMIQUE DANS UN FILM LIQUIDE MINCE SUR UN DISQUE TOURNANT

Résumé—Les résultats d'une simulation numérique de l'écoulement et du coefficient de convection associé sont présentés pour un mince film liquide adjacent à un disque tournant horizontal. Le calcul est conduit pour différentes vitesses de rotation et plusieurs débits en utilisant un système de coordonnées tridimensionnel adapté. Puisque la géométrie de la surface libre est inconnue et dépend du débit, de la vitesse de rotation et des autres paramètres, on utilise une procédure itérative. La hauteur calculée du film s'accorde bien avec les données expérimentales connues. L'écoulement est dominé par l'inertie près de l'entrée et vers la surface libre et il est dominé par le force centrifuge pour les grands rayons et près du disque. La rotation augmente le coefficient de transfert d'une façon très significative.

NUMERISCHE SIMULATION VON STRÖMUNG UND WÄRMEÜBERGANG IN EINEM DÜNNEN FLÜSSIGKEITSFILM AUF EINER ROTIERENDEN SCHEIBE

Zusammenfassung—Für die Strömung eines dünnen Flüssigkeitsfilms auf einer rotierenden Scheibe mit freier Oberfläche werden die Ergebnisse einer numerischen Simulation des Strömungsfelds und der damit verbundenen Wärmeübergangskoeffizienten präsentiert. Die Berechnungen wurden für unterschiedliche Massenströme und Winkelgeschwindigkeiten unter Verwendung eines dreidimensionalen Koordinatensystems mit Ursprung an der Grenzfläche ausgeführt. Die Geometrie der freien Oberfläche ist zunächst unbekannt, da sie vom Massenstrom, der Winkelgeschwindigkeit und anderen Parametern abhängt. Die Position der Grenzfläche muß folglich iterativ ermittelt werden. Die berechnete Filmhöhe stimmt sehr gut mit vorhandenen Meßwerten überein. Die Strömung wird im Bereich des Zulaufs und nahe der freien Oberfläche und der Trägheit bestimmt, wohingegen die Zentrifugalkraft für größere Radien und für Stellen direkt an der Scheibe überwiegt. Der Wärmeübergangskoeffizient wird durch die Rotation wesentlich erhöht.

ЧИСЛЕННОЕ МОДЕЛИРОВАНИЕ ТЕЧЕНИЯ ЖИДКОСТИ И ТЕПЛОПЕРЕНОСА ПРИ ОБТЕКАНИИ ВРАЩАЮЩЕГОСЯ ДИСКА ТОНКОЙ ЖИДКОЙ ПЛЕНКОЙ

Аннотация—Представлены результаты численного моделирования поля течения и коэффициента теплопереноса в случае течения со свободной поверхностью тонкой жидкой пленки, прилегающей к горизонтальному вращающемуся диску. Расчеты для различных расходов и скоростей вращения проводились с использованием трехмерной системы координат, связанной с границей. Поскольку геометрия свободной поверхности неизвестна и зависит от расхода, скорости вращения и других параметров, для орределения ее расположения применялся метод итерации. Результаты расчетов толщины пленки хорошо согласуются с имеющимися экспериментальными данными. Во входном участке и вблизи свободной поверхности течение определялось инерцией, а при больших радиусах и на участках, прилегающих к диску – центробежной силой. Вращение вызывало существенное увеличение коэффициента теплопереноса.